IOPscience iopscience.iop.org

Home Search Collections Journals About Contact us My IOPscience

Room temperature deposition of sputtered TiN films for superconducting coplanar waveguide resonators

This content has been downloaded from IOPscience. Please scroll down to see the full text.

2014 Supercond. Sci. Technol. 27 015009

(http://iopscience.iop.org/0953-2048/27/1/015009)

View the table of contents for this issue, or go to the journal homepage for more

Download details:

IP Address: 128.111.61.7
This content was downloaded on 26/03/2014 at 09:14

Please note that terms and conditions apply.

IOP Publishing Superconductor Science and Technology

Supercond. Sci. Technol. **27** (2014) 015009 (10pp) doi:10.1088/0953-2048/27/1/015009

Room temperature deposition of sputtered TiN films for superconducting coplanar waveguide resonators

S Ohya[1,4], B Chiaro[2], A Megrant[2,3], C Neill[2], R Barends[2], Y Chen[2], J Kelly[2], D Low[2], J Mutus[2], P J J O'Malley[2], P Roushan[2], D Sank[2], A Vainsencher[2], J Wenner[2], T C White[2], Y Yin[2], B D Schultz[1], C J Palmstrøm[1,3], B A Mazin[2], A N Cleland[2] and John M Martinis[2]

[1] Department of Electrical and Computer Engineering, University of California, Santa Barbara, CA 93106-9560, USA
[2] Department of Physics, University of California, Santa Barbara, CA 93106, USA
[3] Department of Materials, University of California, Santa Barbara, CA 93106-9530, USA

E-mail: ohya@cryst.t.u-tokyo.ac.jp and martinis@physics.ucsb.edu

Received 15 June 2013, revised 12 September 2013
Accepted for publication 15 November 2013
Published 5 December 2013

Abstract

We present a systematic study of the properties of room temperature deposited TiN films by varying the deposition conditions in an ultra-high-vacuum reactive magnetron sputtering chamber. By increasing the deposition pressure from 2 to 9 mTorr while keeping a nearly stoichiometric composition of $Ti_{1-x}N_x$ ($x = 0.5$) without substrate heating, the film resistivity increases, the dominant crystal orientation changes from (100) to (111), grain boundaries become clearer, and the strong compressive in-plane strain changes to weak tensile in-plane strain. The TiN films absorb a high concentration of contaminants including hydrogen, carbon, and oxygen when they are exposed to air after deposition. With the target–substrate distance set to 88 mm the contaminant levels increase from ∼0.1% to ∼10% as the pressure is increased from 2 to 9 mTorr. The contaminant concentrations also correlate with in-plane distance from the center of the substrate and increase by roughly two orders of magnitude as the target–substrate distance is increased from 88 to 266 mm. These contaminants are found to strongly influence the properties of TiN thin films. For instance, the resistivity of stoichiometric films increases by around a factor of 5 as the oxygen content increases from 0.1% to 11%. These results strongly suggest that the energy of the sputtered TiN particles plays a crucial role in determining the TiN film properties, and that it is important to precisely control the energy of these particles to obtain high-quality TiN films. Superconducting coplanar waveguide resonators made from a series of nearly stoichiometric films grown at pressures from 2 to 7 mTorr show a substantial increase in intrinsic quality factor from $\sim 10^4$ to $\sim 10^6$ as the magnitude of the compressive strain decreases from nearly 3800 MPa to approximately 150 MPa and the oxygen content increases from 0.1% to 8%. Surprisingly, the films with a higher oxygen content exhibit lower loss, but care must be taken when depositing at room temperature to avoid nonuniform oxygen incorporation, which presents as a radially dependent resistivity and becomes a radially dependent surface inductance in the superconductor.

Keywords: resonator, titanium nitride, TiN, qubit, quantum circuit

(Some figures may appear in colour only in the online journal)

1. Introduction

Superconducting coplanar waveguide (SCPW) resonators are critical elements in circuits that are used for photon

[4] Present address: Department of Electrical Engineering and Information Systems, The University of Tokyo, 7-3-1 Hongo, Bunkyo-ku, Tokyo 113-8656, Japan.

 © 2014 IOP Publishing Ltd Printed in the UK

detection and quantum information processing. One of the most important figures of merit for the SCPW is its intrinsic quality factor Q_i, which governs the energy relaxation time of the resonator. As such, the resonator Q_i is an important indicator of the materials limit of the coherence time of quantum integrated circuits made from superconducting thin films. Because the coherence times of superconducting quantum circuit elements (qubits and resonators) directly impacts the fidelity of algorithms executed by a quantum processor, increasing coherence times is a primary branch of active research within the superconducting qubit community. Recently, there has been a growing interest in titanium nitride (TiN) thin films due to their widely tunable critical temperature T_c, large surface inductance, and ability to produce high Q_i resonators [1–10]. In particular resonator low power Q_i of $\sim 10^6$ and qubit energy decoherence times of ~ 55 μs have been reported with devices made from TiN thin films [11, 12].

Encouraged by observations of high power $Q_i \gtrsim 2 \times 10^7$ and motivated by multilayer device applications that constrain processing conditions, we pursue room temperature deposition that optimizes the low power Q_i [13]. Although excellent performance has been achieved with TiN SCPW resonators, their loss mechanisms are still not clear due to the complex properties of TiN. Complicating the matter, TiN films are known to absorb contaminants when they are exposed to air [14–16]. In fact, a high concentration of oxygen, up to $\sim$20%, has been reported in TiN films [17–19]. Since the contaminants absorbed from the air are strong candidates for two-level systems (TLSs) that can cause degradation in the performance of superconducting devices [20], a systematic investigation of the film quality of TiN is quite important.

Although many studies have been done on TiN since the 1980s, it remains difficult to relate sputtering conditions to the properties of the resulting films and there is little information linking the film properties to the performance of microwave electronic devices made from the films. Here, we show a detailed analysis focusing on stoichiometric $Ti_{1-x}N_x$ films ($x = 0.5$) obtained by adjusting the N_2 flow rate. We show that the kinetic energy of the sputtered TiN particles, which is a function of the pressure, radial position, and target–substrate (T–S) distance, plays a crucial role in determining film properties such as strain, resistivity, grain structure, crystallographic texture, and contaminant levels. We find that the quality factors of resonators made from TiN depend strongly on the material properties of the thin films. Specifically, we find the low power Q_i to be correlated with reduced film strain and increased O content. We find that resonators with a low power $Q_i > 10^6$ can be reliably produced from low film strain TiN.

2. Film preparation

TiN films were deposited by DC reactive magnetron sputtering in an ultra-high-vacuum deposition chamber (AJA International, Inc.) with a background pressure in the lower 10^{-10} Torr range. This system has a high-vacuum load lock chamber connected to the main deposition chamber. We used a 6-in gun with a 99.995% purity, 4-in Ti target. The substrate and target face one another and are centered on a common axis. Ultra-high purity (99.9999%) Ar and N_2 gas sources were introduced to the deposition chamber through Micro Torr purifiers (SAES Pure Gas, Inc.). All depositions were done at room temperature with a fixed Ar flow rate of 15 sccm and with a constant DC plasma power of 600 W. Under these conditions the nominal incident energy of Ar^+ ions on the Ti target is from 350 to 380 eV, depending on the deposition pressure and N_2 flow rate. During deposition, the substrate holder was rotated at $\sim$30 rpm. No substrate bias was applied. We used high-resistivity Si(001) substrates (>10 000 Ω cm, Addison Engineering, Inc.) for all depositions. Before installing a Si substrate in the load lock, the substrate was cleaned with Nano-Strip (Cyantek Corp, Inc.) for 10 min, followed by buffered-HF cleaning for 1 min to remove any native oxide and terminate the Si surface with hydrogen. We installed the Si substrate in the load lock as quickly as possible after cleaning, typically within 45 min. Before deposition of TiN, the Ti target was pre-sputtered for 2 min with the same conditions as for the subsequent TiN deposition. In sections 3–5 of this paper, we used a fixed target–substrate (T–S) distance of 88 mm, whereas in section 6, we investigated the effect of the T–S distance on the properties of the TiN films. Film thicknesses varied from 100 to 900 nm.

3. Basic properties

Figures 1(a)–(c) shows the N_2 flow-rate dependence of the TiN thin film room temperature resistivity, T_c, and composition x, defined as the N content divided by the sum of the Ti and N contents. The film thickness, T_c, and x were measured by scanning electron microscopy (SEM), a physical property measurement system (Quantum Design, Inc.), and Rutherford back scattering (RBS), respectively. Using RBS we can determine the film composition with an error of 1–2%. In the RBS measurements, we detected Ti, N, C, and O signals. We did not see any clear Ar signal, which was previously reported in sputtered TiN films [21]. Resistivity values were measured within several hours of deposition. Although a gradual evolution in the film oxygen content has been reported over the timescale of 100 h after deposition [16], our films only show 7% increase in resistivity one month after deposition, which means that our films are relatively stable. We measured T_c and x several weeks after deposition. Here, the films were deposited on quarter pieces of 3-in Si wafers. All measurements were done near the center of these pieces.

Increasing the N_2 flow rate increases the N concentration on the target surface, which increases x. By comparing figure 1(a) with (c), we see that the resistivity minimum corresponds to the stoichiometric condition ($x = 0.5$) regardless of deposition pressure. This is consistent with previous studies of TiN carried out at a relatively low deposition pressure [22, 23]. Our results show that the resistivity minimum of the resistance versus N_2 flow

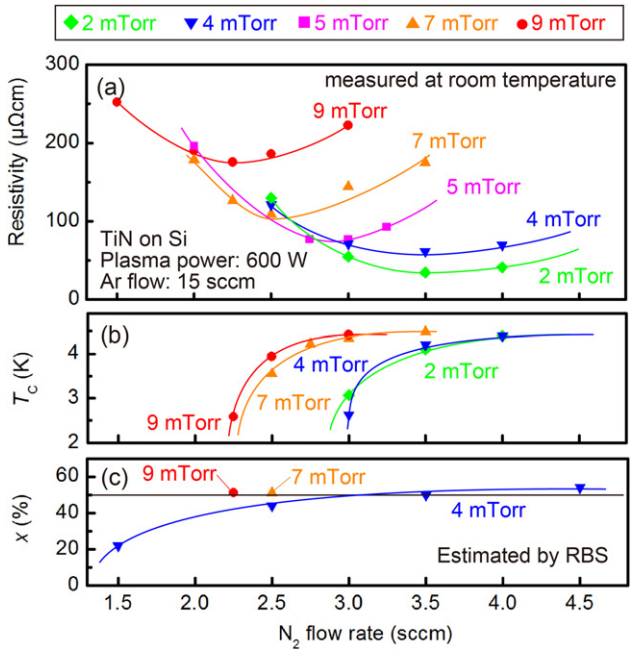

Figure 1. N_2 flow-rate dependence of the (a) room temperature resistivity, (b) T_c, and (c) x of $Ti_{1-x}N_x$ films deposited at 2, 4, 5, 7, and 9 mTorr, where we estimated x by using RBS. The curves are guides for the eyes. All of these depositions were done at room temperature with the Ar flow rate fixed at 15 sccm and the plasma power of 600 W. For the measurements of the resistivity and T_c, the film thickness was ∼200 nm for the TiN films deposited at 2 mTorr and was ∼100 nm for others.

at constant pressure curve is a good indicator of the stoichiometric point even with a high contamination density. This is important because in section 4 it will be shown that resistivity is a strong function of O content which varies from ∼0.1% to ∼10% over this pressure range. We note that the lowest resistivity film obtained in this study was 34.2 $\mu\Omega$ cm. This is a typical value obtained for TiN films deposited at room temperature and slightly higher than single-crystal TiN (18 $\mu\Omega$ cm) [24]. In figure 1(b), T_c increases and saturates at 4.5 K while increasing the N_2 flow rate. As x increases in $Ti_{1-x}N_x$, the dominant phase of the film is changed from Ti_2N, whose T_c is 50 mK, to TiN, with T_c around 5.6 K [25–27]. This phase change can explain the steep change of T_c when $x < 0.5$. In figure 1(b), we see that the T_c of the stoichiometric TiN film decreases by increasing the deposition pressure, which we believe is due to the increase in contaminant concentrations discussed in section 4 (see figure 1 with the N_2 flow rate at 3.5, 3.5, 2.5, and 2.25 sccm when the deposition pressure is 2, 4, 7, and 9 mTorr, respectively).

In figure 1(a), the resistivity rises substantially when increasing the deposition pressure, and the stoichiometric point shifts to a smaller N_2 flow rate. The resistivity increase can be explained by the morphology and contamination changes discussed below. The shift of the stoichiometric point is probably due to the effect of the Ar neutrals reflected from the Ti target to the substrate during sputtering. These neutrals have the same order of mean free path as the sputtered particles [28], and re-sputter the TiN film surface during the

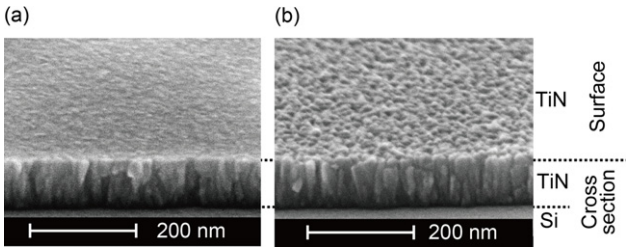

Figure 2. SEM images of the stoichiometric TiN films deposited at (a) 2 and (b) 9 mTorr. The incident SEM electron-beam direction is tilted by 70° from the film-surface normal.

deposition. It is known that the film surface is always covered with a stable N-rich TiN thin layer due to the high reactivity of atomic N, which has an important role in determining the N content of the film. When the reflected Ar neutrals have a high energy at a low deposition pressure, re-sputtering by the Ar neutrals removes this N-rich surface. However, at high pressure, this effect becomes less important due to the higher collision probability of the Ar neutrals, so stoichiometric TiN is obtained at a smaller N_2 flow rate as the deposition pressure increases [29].

4. Properties of stoichiometric films

In this section, we focus on nearly stoichiometric $Ti_{1-x}N_x$ films ($x \simeq 0.5$). Films were deposited by setting the N_2 flow rate at 3.5, 3.5, 3.0, 2.5, and 2.25 sccm when the deposition pressure was 2, 4, 5, 7, and 9 mTorr, respectively. These N_2 flow rates correspond to the resistivity minimum points in figure 1(a). We fixed the Ar flow rate at 15 sccm and the T–S distance at 88 mm.

Figures 2(a) and (b) show SEM images of the stoichiometric TiN films for deposition pressures of 2 and 9 mTorr, respectively. The incident electron-beam direction is tilted by 70° from the film-surface normal. These images were taken near the center of the substrates (quarter pieces of 3-in Si wafers). We see that these TiN films are polycrystalline with columnar grains. In the film deposited at 2 mTorr, these grains are intimately bound to their neighbors. In contrast, in the film deposited at 9 mTorr, the grain boundaries are clear, and the surface is rough. The grain boundaries seen in (b) are thought to allow contaminants into the film, which is consistent with the increase in the C + O concentration from 0.3% at 2 mTorr to 13.5% at 9 mTorr, as shown in table 1.

The morphology change due to the pressure increase is similar to the effect of the application of a substrate bias, which has been well studied previously [14]. The grains tend to bind as the negative substrate-bias voltage becomes larger. It is known that the atomic peening mechanism leads to a dense structure (as in figure 2(a)), where the gas atoms reflected from the target with a high momentum pack together the sputtered atoms and increase the density of atoms in each column [30]. This effect is more significant at lower pressure, where the reflected atoms have higher momenta. The higher momentum of the sputtered particles at a lower pressure also can help to make such a dense structure.

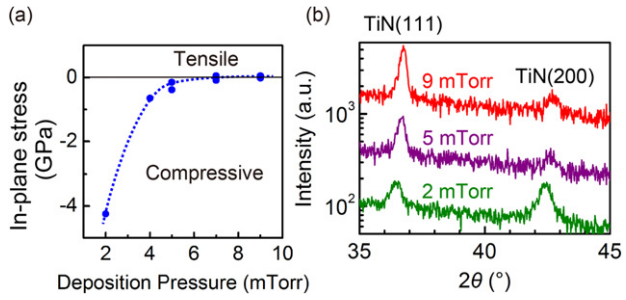

Figure 3. (a) Stress measured in the stoichiometric TiN films as a function of the deposition pressure. The stress values shown here were measured at the center of 3-in wafers. (b) The ω–2θ x-ray diffraction scans of 200-nm-thick stoichiometric TiN(111) films deposited at 2, 5, and 9 mTorr (from bottom to top).

Table 1. Ar and N_2 flow rates used to deposit nearly stoichiometric TiN films, and the concentrations of C and O relative to the sum of the Ti and N contents. The C and O concentrations were estimated from SIMS intensities integrated over the film thickness, using RBS data of the TiN film deposited at 9 mTorr as a reference.

	Flow rate (sccm)		Concentration (%)	
Pressure (mTorr)	Ar	N_2	C	O
2	15	3.5	0.2	0.1
4	15	3.5	0.9	0.6
7	15	2.5	3.6	8
9	15	2.25	2.5	11

The relatively high-atomic-density TiN columns obtained in a low pressure deposition generate a large stress in the film. Figure 3(a) shows the deposition pressure dependence of the in-plane stress in 100-nm thick stoichiometric TiN films. The strain values were determined with a wafer bow measurement (FLX-2320, KLA Tencor, Inc.) at the center of the TiN films deposited on 3-in Si wafers at room temperature. When the deposition pressure is low, the film has a strong in-plane compressive strain. By increasing the deposition pressure, the in-plane strain is reduced and changes to a weak tensile strain. This is a very common feature in films deposited by sputtering and is consistent with the SEM results shown in figure 2.

Figure 3(b) shows x-ray diffraction ω–2θ scans of the 200-nm-thick stoichiometric TiN films deposited at 2, 5, and 9 mTorr (from bottom to top). In all the spectra, we see two peaks at ∼36.5° and ∼42.5° corresponding to the TiN(111) and (200) planes, respectively. The only other peaks detected in our stoichiometric TiN films were from the Si substrate. With increasing pressure, these TiN peaks shift toward larger angles, and the (111) peak becomes sharper. The lattice constants in the surface-normal direction estimated from these peaks are 0.4260 nm at 2 mTorr and 0.4237 nm at 9 mTorr (corresponding to a 0.5% decrease in the lattice constant). Since the intrinsic lattice constant of TiN is 0.424 nm, these values are consistent with the tendency of the stress to change as seen in figure 3(a).

By increasing the deposition pressure, the dominant crystal orientation changes from (200) to (111). As the mobility of the adatoms is increased by decreasing the deposition pressure, they tend to make closer-packed structures. Thus, the high adatom mobility causes the crystal growth along the (200) orientation, which has the lowest surface free energy [31].

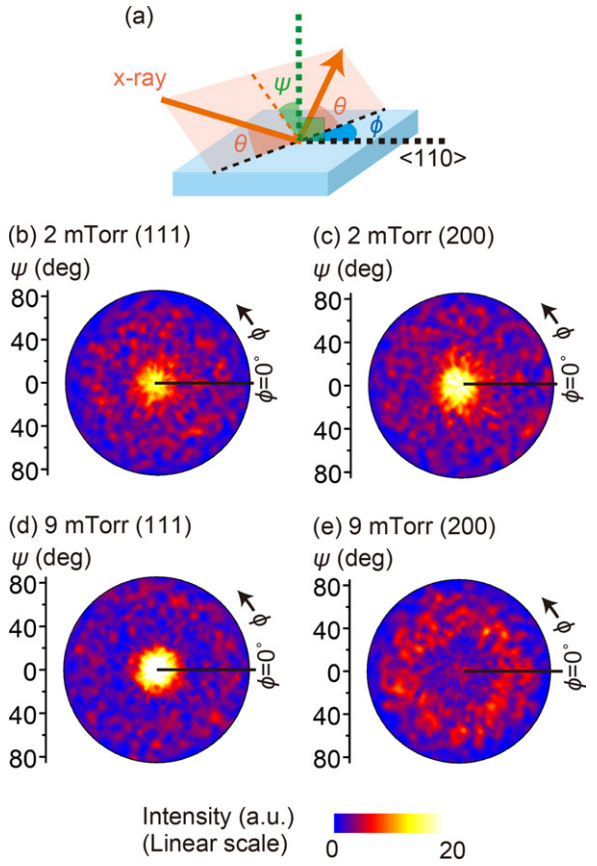

Figure 4. (a) Schematic x-ray beam alignment in our texture measurements. (b), (c) Results of the texture measurements on the stoichiometric TiN film deposited at 2 mTorr when θ is fixed at (b) 36.66° and (c) 42.61°. (d), (e) The same measurement results when the deposition pressure is 9 mTorr.

We carried out x-ray texture measurements on the 200-nm-thick stoichiometric TiN films, which give us a more complete understanding of the crystallinity of these films. Figure 4(a) shows the schematic x-ray beam alignment in our measurements. We define ϕ as the in-plane angle between the Si in-plane ⟨110⟩ axis and the x-ray beam plane (the pink plane in figure 4(a)), whereas ψ expresses the angle between the measurement direction (broken orange line) and the surface normal of the film. Figures 4(b) and (c) show the measurement results of the TiN films deposited at 2 mTorr, when θ is fixed at 36.66° corresponding to TiN(111), and at 42.61° corresponding to TiN(200), respectively. We see that the (111) and (200) planes are nearly parallel to the film surface (corresponding to the center yellow zones). The ψ direction of these planes fluctuates slightly ($\psi = 0°$–$20°$). As can be seen in the SEM image of figure 2(a), the growth directions of the grains are not perfectly aligned in the surface-normal direction but have some fluctuation, so these ψ distributions observed in the x-ray texture measurements are probably due to these grains' tilt. In addition, we see that

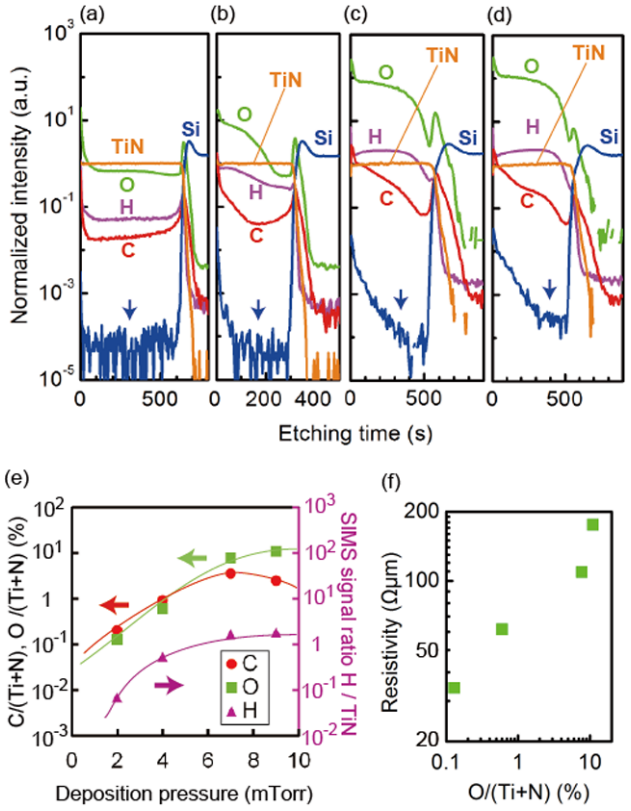

Figure 5. SIMS depth profile of the stoichiometric TiN films deposited at (a) 2 mTorr, (b) 4 mTorr, (c) 7 mTorr, and (d) 9 mTorr as a function of the Ar^+ etching time from the surface toward the Si substrate. We show the SIMS signals of the H, C, O, Si, and TiN. Here, all the signals are normalized by the intensity of TiN in the TiN-layer region. (e) Deposition pressure dependence of the concentrations of H, C and O. Since it is difficult to determine the H content, we plot the integrated SIMS intensity of H over the thickness divided by that of TiN. The actual concentrations of C and O were estimated from the total SIMS signals in (a)–(d) using the RBS data of the TiN film deposited at 9 mTorr as a reference. (f) The dependence of resistivity on O content for the nearly stoichiometric TiN films.

there are randomly oriented (111) and (200) planes (many red areas). Figures 4(d) and (e) show the same measurement results on the TiN film deposited at 9 mTorr. In this case, (111) planes nearly parallel to the film surface become dominant. The (200) planes observed at $\psi = 40°$–$70°$ are thought to be the same crystal phase with the (111) plane observed at the center in (d). From these results, we see that the (111) plane is selectively grown in the growth direction in the high pressure condition with a ψ fluctuation up to $\sim 20°$.

Figures 5(a)–(d) shows the secondary ion mass spectroscopy (SIMS) results from the TiN films deposited at 2, 4, 7, and 9 mTorr. The thicknesses of these films are 200, 100, 100, and 100 nm, respectively. These TiN films were deposited on quarter pieces of 3-in Si substrates. We etched the film from the surface toward the Si substrate with different etching rates depending on the sample. The Si interface is identified by the increase in the Si signal. Here, all the signals are normalized by the intensity of TiN in the TiN-layer region in each graph. Thus, we can directly compare the relative concentrations between the samples. We note that the low level signals of Si in the TiN layer (see the arrows) are not coming from Si, but probably coming from a contaminant that has the same mass number (29) as is used to detect Si, such as COH. The concentrations of H, C, and O strongly increase with increasing deposition pressure. The TiN films incorporate the contaminants when they are exposed to air after deposition [16]. We have observed this directly by witnessing the films change color from the golden color of stoichiometric TiN to the green color of titanium oxynitride [32] as the load lock is being vented.

From our RBS measurements on the 100-nm thick TiN film deposited at 9 mTorr, C and O contents relative to the sum of the Ti and N contents are estimated to be 2.5% and 11%, respectively. Using these values and integrating the SIMS intensities shown in figures 5(a)–(d), we can estimate the contamination levels of C and O as shown in table 1. The deposition pressure dependence of these concentrations is shown in figure 5(e). As shown in figure 1, the resistivity increases and T_c decreases as the deposition pressure is increased; this change is likely due to rising contaminant levels in the TiN. In figure 5(f) we show the strong dependence of resistivity on oxygen content, indicating that the regulation of oxygen content is essential to the control of the electronic properties of the film.

As shown in figure 2, the grain boundaries become more defined as the deposition pressure increases, and the surface area, which can absorb the contaminants, becomes larger as a consequence. It has been reported that x-ray photoemission spectroscopy measurements on sputtered TiN films show a Ti $2p_{3/2}$ peak at 458 eV which corresponds to TiO_2 [16], which suggests that some of the O atoms may enter the TiN crystal and react with Ti atoms. Under high pressure conditions, bonds between Ti and N become weak due to the low kinetic energy of the sputtered particles, which is also thought to be the origin of such a high level of contaminants in the TiN films deposited at high pressure.

5. In-plane distribution

As shown above, the TiN film properties directly depend on the kinetic energy of the sputtered particles, which can be controlled by deposition pressure. In magnetron sputtering, the in-plane energy distribution of the sputtered particles is inevitable because there is an in-plane inhomogeneity of the plasma intensity caused by the spatial variation of the magnetic field from the magnetron. Figure 6(a) shows the cross-sectional SEM images of a stoichiometric TiN film deposited on a 3-in Si(001) wafer at 7 mTorr. We show the images taken at 6–35 mm from the center of the wafer. There is a similar tendency seen in the pressure dependence; the grain boundary becomes clearer from the center to the edge. In figure 6(b), we show the measured sheet resistance R_{sheet} (blue circles) and the film thickness (red triangles) as a function of the distance from the center of the wafer. We see that the film thickness is reduced by 5% from 890 to 850 nm, whereas, R_{sheet} increases by 70% from 1.5 to 2.5 Ω. This large increase

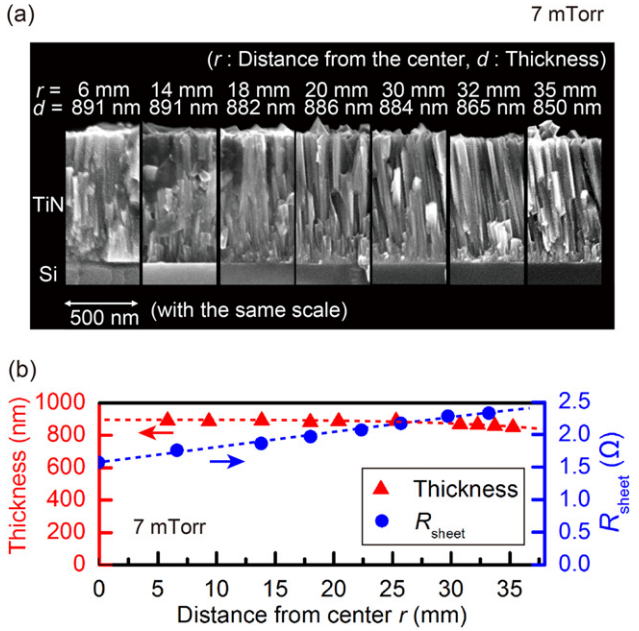

Figure 6. (a) Cross-sectional SEM images of the stoichiometric TiN film deposited at 7 mTorr on a 3-in Si(001) wafer. Here, we show the images taken at positions from 6 to 35 mm measured from the center of the wafer. (b) R_{sheet} (red triangles) and film thickness (blue circles) as a function of the distance from the center of the wafer.

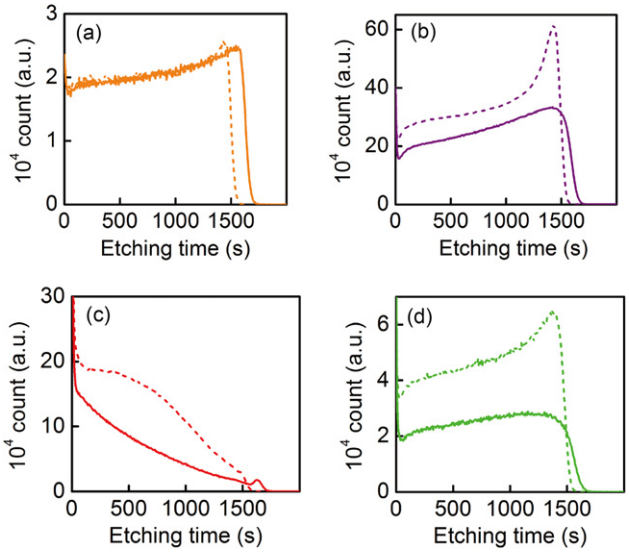

Figure 7. SIMS depth profiles of (a) TiN, (b) H, (c) C, and (d) O obtained in the stoichiometric TiN film deposited at 7 mTorr. The solid curves are those at the center, and the dotted curves are the ones at the edge of the 3-in wafer.

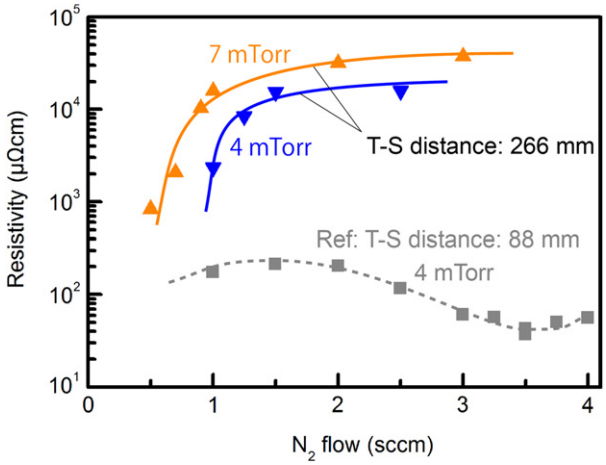

Figure 8. The orange (triangle) and blue (inverse triangle) points are the resistivities of the TiN films as a function of the N_2 flow rate when the *T*–*S* distance is 266 mm and the deposition pressure is 7 and 4 mTorr, respectively. As a reference, we show data for films deposited at 4 mTorr with the *T*–*S* distance at 88 mm (gray rectangles), which is the same *T*–*S* distance used for all the depositions of the TiN films shown in sections 3–5. The solid and the broken curves are guides for the eyes.

in R_{sheet} cannot be explained by the 5% thickness reduction alone.

Figures 7(a)–(d) shows the SIMS depth profiles of TiN, H, C, and O on the stoichiometric TiN film deposited at 7 mTorr. The solid curves are the SIMS intensities at the center, and the dotted curves are the ones at the edge of the 3-in wafer. Here, we show the raw data. We see that the TiN contents are the same between at the center and at the edge. However, all the contaminant levels are higher at the edge than those at the center. This suggests that the in-plane energy distribution of the sputtered particles causes the large distribution of the resistance as well as the contamination.

6. *T*–*S* distance dependence

The energy of the sputtered particles just before reaching the film surface also depends on the *T*–*S* distance. The sputtered particles experience more collisions for larger *T*–*S* distances. Here, we studied the effect of the *T*–*S* distance on film quality. The orange (triangle) and blue (inverse triangle) points in figure 8 show the resistivities of the TiN films as a function of the N_2 flow rate when the *T*–*S* distance was 266 mm and the deposition pressure was 7 and 4 mTorr, respectively. As a reference, we show the films deposited at 4 mTorr with a *T*–*S* distance of 88 mm (the same *T*–*S* distance as was used for all depositions of the TiN films shown in the previous sections). The resistivity becomes two orders of magnitude higher as the *T*–*S* distance is changed from 88 to 266 mm. The films deposited with a large *T*–*S* distance (266 mm) have a green color, which is the typical color of titanium oxynitride (TiNO). By carrying out RBS analysis on the film deposited at 7 mTorr with a N_2 flow rate of 3 sccm and a *T*–*S* distance of 266 mm, the carbon and oxygen contents are estimated to be 5% and 27%, respectively. We found that the color of these films was gold just after the deposition when they are still in the vacuum chamber. However, while venting the load lock with N_2 gas (purity: 99.999%) with TiN samples inside, the film color was observed to change from gold to green. This shows that the grain boundary surfaces of the TiN films are highly reactive since H, C, and O were gettered from the nearly pure N_2. This result indicates that TiN films deposited with low sputtered-energy particles absorb a high amount of these

contaminants, and the contaminant levels strongly depend on the sputtered particle energy. Therefore, the T–S distance is important for the production of high-quality TiN films [33].

7. Properties of the SCPW resonators

The application of superconducting films to circuits that detect photons and process quantum information motivates our investigation of the relationships between deposition conditions and the properties of the obtained material. Coupling this knowledge with an understanding of the impact that these materials properties have on device performance enables the realization of thin films optimized for quantum circuits. Whereas in the previous sections we discussed the response of TiN thin films to the reactive sputtering parameters used in their production, here we inspect the influence of specific TiN film features on the performance characteristics of devices into which the films are made. In order to evaluate these effects, we have deposited a series of nearly stoichiometric thin films at several pressures (2, 4, 5, and 7 mTorr) using the procedure outlined in the preceding sections with a T–S distance of 88 mm. Next, we patterned these films into SCPW microwave resonators and compared the performance of these devices to the material properties of either an unprocessed section of the same sample or of a companion wafer deposited under nominally identical conditions. The resonators in our experiment take the form of a quarter wavelength segment of coplanar waveguide terminated at opposite ends by an electrical open circuit and short circuit to the ground plane.

Among the virtues of the SCPW resonator is the simplicity of its fabrication. The SCPW resonator thus provides a context for our study of material versus device performance that is protected against the conflation of fundamental material data and complications arising from involved cleanroom proceedings. In this experiment, the substrate preparation and deposition described previously were followed by a single optical lithography and etching sequence. The nominally 100 nm TiN films were etched in an inductively coupled plasma etcher with Cl_2 as the reactive species, under conditions yielding an etch rate of approximately 5.5 nm s^{-1}. This primary etch was followed with a secondary, 5 s SF_6 etch, as this has been shown to reduce loss [34]. This reliably produced a SCPW structure with a silicon substrate trench depth of 56 ± 11 nm. Once etched, the wafers were diced to yield chips measuring 6.25 mm $\times$ 6.25 mm square. Dies drawn from the center regions of our wafers were packaged in an Al sample box with an approximate linear wirebond density of 3 mm^{-1} from the box to the device ground plane, in preparation for measurement.

During measurement, the sample box was mounted on the cold plate of an adiabatic demagnetization refrigerator with a base temperature of ~70 mK. This cold plate is shielded in stages from infrared radiation and external magnetic fields [35]. The output of the test chip was connected to a high-electron-mobility transistor amplifier at 4 K, followed by a room temperature amplifier chain. A vector network analyzer (Agilent 5230A or 5242A) was used for excitation and detection. We characterized the SCPW by measuring the transmission scattering parameter S_{21} of a microwave transmission line capacitively coupled to a resonator. Details of the measurement and analysis are supplied by Megrant *et al* [36].

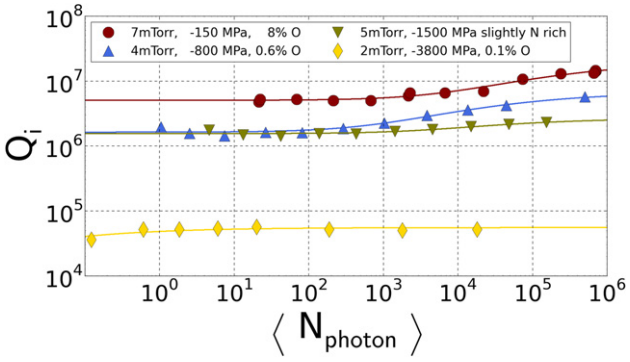

Figure 9. The power dependence of the SCPW resonator Q_i for the nearly stoichiometric films deposited at 2, 4, 5, and 7 mTorr and respective strain values −3800, −800, −1500, and −150 MPa, expressed in terms of the expectation value of the resonator's photonic occupation number. The solid line is a fit to the expected TLS loss power dependence.

Because energy relaxation events form an important error class in quantum information processing, this study focused on maximizing the low power Q_i, which is generally agreed to be limited by coupling to TLSs in the low energy excitation regime that is relevant to quantum computing and accessed in the limit where the number of photons in the resonator is small. Figure 9 reports the dependence of Q_i on the microwave drive power for devices made from the nearly stoichiometric films deposited at 2, 4, 5, and 7 mTorr with N_2 flow rates of 3.5, 3.5, 3.5, and 2.5 sccm, which had compressive film strain values of 3800, 800, 1500, and 150 MPa, respectively. The 5 mTorr sample was deposited under slightly nitrogen-rich conditions and we believe that this explains the slight nonmonotonicity of film strain vs deposition pressure for these samples. For figure 9 we have selected the best performing device from each sample to establish an upper bound on device performance for a given set of material parameters, independent of such systematic issues as cleanroom process variability and time dependent external magnetic fields. We note that Q_i is enhanced as the film strain decreases and the oxygen content increases. In particular, the lowest strain film produced a resonator with a low power $Q_i = 5.0 \times 10^6$, the highest reported low power value to date.

Since the contamination of these TiN films plays a significant role in determining their properties, it is worthwhile to comment on the reproducibility of these results. For this reason figure 10 displays the internal quality factors of all devices measured in the low power regime. The low power Q_i value in figure 10 is that obtained by fitting the power dependence of the resonator Q_i to a TLS loss model [37] and evaluating this fit at $\langle N_{photon} \rangle = 1$. Focusing on the nearly stoichiometric series deposited at 2, 4, 5, and 7 mTorr, we

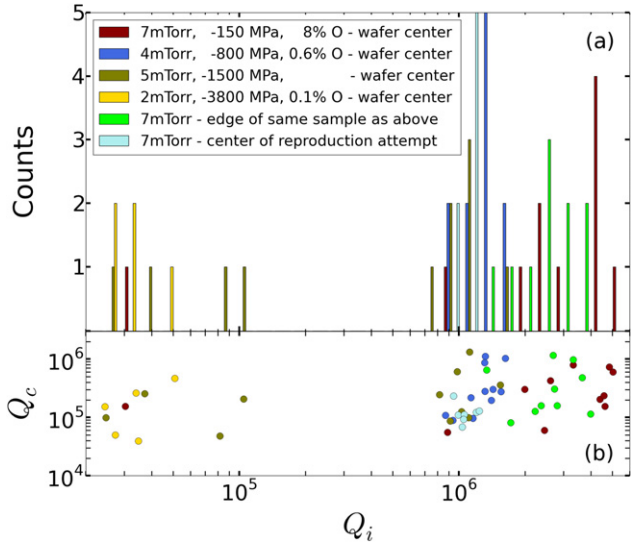

Figure 10. (a) A histogram reporting the low power Q_i, obtained by evaluating a fit to the TLS model loss power dependence at $\langle N_{photon} \rangle = 1$. Data shown are for the nearly stoichiometric films deposited at 2, 4, 5, and 7 mTorr. Also shown are the low power Q_i for resonators at the edge of 7 mTorr high Q_i sample and for resonators from the center of a second sample grown under nominally identical conditions. (b) The measured values of Q_c for the Q_i in (a) show no correlation.

point out that the trend of increasing Q_i with decreasing film strain is present both in the maximum Q_i values achieved, as shown in figure 9, and also for the distributions as a whole. This strongly suggests a strain dependent loss mechanism favoring lower strain films. Looking more broadly at the low power Q_i distribution, we also underscore the reliability of producing resonators with Q_i greater than 1×10^6 over a wide range of deposition conditions, consequent materials properties, and contamination levels. Films with Q_i in this range are valuable to many applications, and the ability to produce such films with a room temperature deposition method is a useful capability because it allows for greater compatibility with multilayer device fabrication.

Since there is a large change in film composition and resistivity between the center and the edge of the wafer, we compare the low power quality factors of resonators made at the edge with resonators made at the center of the lowest strain sample included in our study. We find that while the average edge resonator low power Q_i is slightly lower than that of center resonators, it is a statistically significant improvement over even mildly strained films.

Also shown in figure 10 are the Q_i for a film grown under nominally identical conditions to the 7 mTorr low strain sample. The Q_i of $\sim 1 \times 10^6$ achieved with this film is a very respectable result despite the fact that it was lower than the original. We interpret this result to indicate that at the $Q_i \sim$ several $\times 10^6$ level the resonators may be highly sensitive to the details of the surface preparation and deposition. We posit that a small drift in the deposition chamber or measurement refrigerator conditions may have created a subtle difference in the film properties or electrodynamic response, since this sample was deposited and measured months after the original series.

Because we are reporting very high-quality factors in the low strain films, figure 10(b) also shows the coupling quality factor Q_c. We call attention to the fact that for the two highest Q_i measured (5.0×10^6 and 4.8×10^6) the Q_c were 6.0 and 7.4×10^5. As seen in figure 10 typical Q_c in these measurements were in the 10^5 to 10^6 range, making the Q_c values appropriate for Q_i that we are reporting.

Taken together, $Q_i \gtrsim 1 \times 10^6$ is a very reliable, reproducible capability of TiN films grown at room temperature even with contamination. At the high end we observe low power quality factors of up to 5 million, arising from a film that was measured to have 8% oxygen and 4% carbon. For groups prioritizing a room temperature deposition process over tight uniformity tolerance, the films produced with our method have proven to have reliably high performance albeit with certain limitations. For applications requiring room temperature deposition and a maximum low power Q_i our results provide convincing evidence that strain minimization is an important aspect of optimization.

Since surface oxides of superconducting electrodes and their substrates are supposed to harbor the TLS populations [38] responsible for limiting the low power quality factors of SCPWs, the result that increased oxygen concentration in our compound superconducting films is associated with an increase in quality factor was not expected. More surprising, perhaps, is the absolute magnitude of the oxygen concentration; in the best performing films the ratio of O to TiN was measured to be 8%. We interpret this result to suggest that the presence of oxygen is not, in and of itself, deleterious to the resonator quality factor. Rather, oxygen incorporation by the TiN crystal may be an innocuous byproduct of the low strain condition which we suspect is itself fundamentally responsible for the quality factor increase in our experiment.

Although significant oxygen impurity concentrations in our TiN films do not directly translate to increased loss in our microwave resonators, the presence of oxygen in the TiN crystal is not inconsequential. As seen in figure 5(f), the normal state resistivity of our films depends strongly on the oxygen content. From a SCPW resonator perspective, the salient consequence of increased resistance is a resonant frequency reduction via kinetic inductance augmentation. This is a large effect in TiN, where the kinetic inductance is often larger than the geometric inductance for common device geometries. Applying these facts to the uniformity data in figure 6(b) creates an engineering consideration for those who would make quantum integrated circuits from reactively sputtered TiN deposited at room temperature: The radial dependence of the sputtered TiN particle energy common to many magnetron systems may result in a radial dependence of the oxygen content and through it resistivity, which complicates the design of larger circuits even though the intrinsic loss of the film remains quite low. We remind the reader that if resistance and composition uniformity is a rigid requirement, methods such as planetary motion are available to achieve it.

8. Summary

We have shown a detailed picture of the properties of TiN films deposited at room temperature by varying the deposition pressure and the N_2 flow rate. When fixing the deposition pressure, the resistivity minimum corresponds to the stoichiometric point ($x = 0.5$). By increasing the deposition pressure, while keeping $x = 0.5$, the resistivity rises and T_c decreases. The strong in-plane compressive stress changes to weak tensile stress as the deposition pressure increases. The dominant crystal orientation changes from (200) to (111). The grain boundaries become clearer, and the contamination levels, including H, C, and O, significantly increase. The grain boundaries play a crucial role in the absorption of the contaminants. This morphology change is thought to be induced by the energy change of the sputtered particles due to the change of the deposition pressure.

The in-plane particle energy distribution caused by the in-plane inhomogeneity of the plasma leads to a large radial resistivity change (70%) across a TiN film deposited at 7 mTorr on a 3-in wafer. From the center to the edge of this sample, the grain boundaries become clearer, which is very similar to the effect of deposition pressure increase. We have found that larger amounts of the contaminants H, C, and O exist at the edge of the wafer than at the center. By increasing the *T*–*S* distance from 88 to 266 mm, the film color was changed from gold to green, and we detected a higher amount of H, C, and O in the film deposited with the *T*–*S* distance at 266 mm than at 88 mm. The energy of the sputtered particles, which decreases with distance from the substrate center and with increasing the *T*–*S* distance, is also responsible for these phenomena.

Following the method developed in section 3 of this paper, we deposited nearly stoichiometric films at 2, 4, 5, and 7 mTorr and found that increasing the deposition pressure decreased the film strain and increased the oxygen content. These changes were associated with an increase in the Q_i factor of SCPW resonators made from these films. However, the film resistivity is a strong function of oxygen content and was found to vary considerably with distance from the center of the substrate. The variation in resistivity, which translates to a surface inductance variation in the superconductor, is important to consider in the design and production of larger circuits. However, the resonator performance achieved with TiN makes this material is immediately useful, especially for smaller circuits, even though the precise film composition and resistivity may exhibit a spatial nonuniformity if care is not taken to avoid this condition.

Acknowledgments

We thank M R Vissers, H Sukegawa, and H G Leduc for the technical advice regarding the sputtering of TiN. S O acknowledges the Japan Society for the Promotion of Sciences (JSPS) for a Postdoctoral Fellowship for Research Abroad. Devices were made at the UC Santa Barbara Nanofabrication Facility, a part of the NSF-funded National Nanotechnology Infrastructure Network. This research was funded by the Office of the Director of National Intelligence (ODNI), Intelligence Advanced Research Projects Activity (IARPA), through Army Research Office Grant No. W911NF-09-1-0375. All statements of fact, opinion or conclusions contained herein are those of the authors and should not be construed as representing the official views or policies of IARPA, the ODNI, or the US Government.

References

[1] Sage J M, Bolkhovsky V, Oliver W D, Turek B and Welander P B 2011 *J. Appl. Phys.* **109** 063915
[2] Vissers M R, Kline J S, Gao J, Wisbey D S and Pappas D P 2012 *Appl. Phys. Lett.* **100** 082602
[3] Diener P, Leduc H G, Yates S J C, Lankwarden Y J Y and Baselmans J J A 2012 *J. Low Temp. Phys.* **167** 305
[4] Mazin B A, Bumble B, Meeker S R, O' Brien K, McHugh S and Langman E 2012 *Opt. Express* **20** 1503
Diener P, Schellevis H and Baselmans J J A 2012 *Appl. Phys. Lett.* **101** 252601
[5] Cecil T, Miceli A, Gades L, Datesman A, Quaranta O, Yefremenko V, Novosad V and Mazin B 2012 *Phys. Procedia* **37** 697
[6] Noroozian O, Day P K, Eom B H, LeDuc H G and Zmuidzinas J 2012 *IEEE Trans. Microw. Theory* **60** 1235
[7] Calvo M *et al* 2012 *J. Low Temp. Phys.* **167** 379
[8] Eom B H, Day P K, LeDuc H G and Zmuidzinas J 2012 *Nature Phys.* **8** 623
[9] Krockenberger Y, Karimoto S, Yamamoto H and Semba K 2012 *J. Appl. Phys.* **112** 083920
[10] Driessen E F C, Coumou P C J J, Tromp R R, de Visser P J and Klapwijk T M 2012 *Phys. Rev. Lett.* **109** 107003
[11] Vissers M R, Gao J, Wisbey D S, Hite D A, Tsuei C C, Córcoles A D, Steffen M and Pappas D P 2010 *Appl. Phys. Lett.* **97** 232509
[12] Chang J B *et al* 2013 *Appl. Phys. Lett.* **103** 012602
[13] Leduc H G *et al* 2010 *Appl. Phys. Lett.* **97** 102509
[14] Kumar N, McGinn J T, Pourrezaei K, Lee B and Douglas E C 1988 *J. Vac. Sci. Technol.* A **6** 1602
[15] Mandl M, Hoffmann H and Kücher P 1990 *J. Appl. Phys.* **68** 2127
[16] Logothetidis S, Meletis E I, Stergioudis G and Adjaottor A A 1999 *Thin Solid Films* **338** 304
[17] Radecka M, Pamula E, Trenczek-Zajac A, Zakrzewska K, Brudnik A, Kusior E, Kim-Ngan N-T H and Balogh A G 2011 *Solid State Ion.* **192** 693
[18] Chappe J-M, Martin N, Lintymer J, Sthal F, Terwagne G and Takadoum J 2007 *Appl. Surf. Sci.* **253** 5312
[19] Chowdhury R, Vispute R D, Jagannadham K and Narayan J 1996 *J. Mater. Res.* **11** 1458
[20] Martinis J M *et al* 2005 *Phys. Rev. Lett.* **95** 210503
[21] Williams D S, Baiocchi F A, Beairsto R C, Brown J M, Knoeli R V and Murarka S P 1987 *J. Vac. Sci. Technol.* B **5** 1723
[22] Ahn K Y, Wittmer M and Ting C Y 1983 *Thin Solid Films* **107** 45
[23] Schiller S, Beister G and Sieber W 1984 *Thin Solid Films* **111** 259
[24] Johansson B O, Sundgren J-E and Greene J E 1985 *J. Vac. Sci. Technol.* A **3** 303
[25] Wriedt H A and Murray J L 1987 *Bull. Alloy Phase Diagr.* **8** 378
[26] Vissers M R, Gao J, Kline J S, Sandberg M, Weides M P, Wisbey D S and Pappas D P 2013 *Thin Solid Films* **548** 485
[27] Penilla E and Wang J 2008 *J. Nanomater.* **2008** 267161
[28] Lu J and Lee C G 2011 *Vacuum* **86** 1134

[29] Adjaottor A A, Meletis E I, Logothetidis S, Alexandrou I and Kokkou S 1995 *Surf. Coat. Technol.* **76/77** 142
[30] Thornton J A and Hoffman D W 1985 *J. Vac. Sci. Technol.* **3** 576
[31] Patsalas P, Charitidis C and Logothetidis S 2000 *Surf. Coat. Technol.* **125** 335
[32] Barhai P K, Kumari N, Banerjee I, Pabi S K and Mahapatra S K 2010 *Vacuum* **84** 896
[33] LeDuc H G and Bumble B private communication
[34] Sandberg M, Vissers M R, Kline J S, Weides M, Gao J, Wisbey D S and Pappas D P 2012 *Appl. Phys. Lett.* **100** 262605
[35] Barends R *et al* 2011 *Appl. Phys. Lett.* **99** 113507
[36] Megrant A *et al* 2012 *Appl. Phys. Lett.* **100** 113510
[37] Wang H *et al* 2009 *Appl. Phys. Lett.* **95** 233508
[38] Gao J, Daal M, Vayonakis A, Kumar S, Zmuidzinas J, Sadoulet B, Mazin B A, Day P K and Leduc H G 2008 *Appl. Phys. Lett.* **92** 152505